REAL-TIME ATTITUDE-INDEPENDENT THREE-AXIS MAGNETOMETER CALIBRATION*

John L. Crassidis† and Kok-Lam Lai‡
Department of Mechanical & Aerospace Engineering
University at Buffalo, State University of New York
Amherst, NY 14260-4400

Richard R. Harman§
Flight Dynamics Analysis Branch
NASA Goddard Space Flight Center
Greenbelt, MD 20771

ABSTRACT

In this paper new real-time approaches for three-axis magnetometer sensor calibration are derived. These approaches rely on a conversion of the magnetometer-body and geomagnetic-reference vectors into an attitude independent observation by using scalar checking. The goal of the full calibration problem involves the determination of the magnetometer bias vector, scale factors and non-orthogonality corrections. Although the actual solution to this full calibration problem involves the minimization of a quartic loss function, the problem can be converted into a quadratic loss function by a centering approximation. This leads to a simple batch linear least squares solution. In this paper we develop alternative real-time algorithms based on both the extended Kalman filter and Unscented filter. With these real-time algorithms, a full magnetometer calibration can now be performed on-orbit during typical spacecraft mission-mode operations. Simulation results indicate that both algorithms provide accurate integer resolution in real time, but the Unscented filter is more robust to large initial condition errors than the extended Kalman filter. The algorithms are also tested using actual data from the Transition Region and Coronal Explorer (TRACE).

INTRODUCTION

Three-axis magnetometers (TAMs) are widely used for onboard spacecraft operations. The basic concept behind these devices is a fairly simple one, involving a simple magnetic sensor coupled with an electronics unit to provide data in a digital format. These sensors are useful since they provide both the direction and magnitude of the magnetic field; they are lightweight, reliable, and have low power requirements, with no moving parts.[1] For these reasons most low-Earth orbiting spacecraft (below 1000 km) have TAMs as part of their basic sensor package. It is well known that a TAM can be used to determine a three-axis attitude when coupled with gyros or a dynamic model in an extended Kalman filter.[2] Attitude-knowledge accuracies of 1-2 degrees are common using this

*This research was supported by NASA Goddard Space Flight Center Grant NAG5-12179.
†Associate Professor. E-mail: johnc@eng.buffalo.edu
‡Graduate Student. E-mail: klai2@eng.buffalo.edu
§Aerospace Engineer. E-mail: richard.r.harman@nasa.gov

approach, which can be improved by using well-calibrated sensors to achieve accuracies of 0.1-0.5 degrees.[3] An exciting new area of research involves using a TAM together with rate and sun sensor measurements for orbit (position) estimation. Accuracies on the order of 10 to 100 km can be achieved, which is within the position-knowledge requirements of many spacecraft.[4,5] These studies clearly show that an integrated magnetometer-based attitude/orbit estimation system can provide the necessary knowledge requirements of a spacecraft in a single package.

A paramount issue to the attitude accuracy obtained using magnetometer measurements is the precision of the onboard calibration. The accuracy obtained using a TAM depends on a number of factors, including: biases, scale factors and non-orthogonality corrections. Scale factors and non-orthogonality corrections occur because the individual magnetometer axes are not orthonormal, typically due to thermal gradients within the magnetometer or to mechanical stress from the spacecraft.[6] We should note that even with perfectly calibrated (and noise-free!) magnetometers, inaccuracies still exist due to modelling uncertainty in the Earth's geomagnetic field. These errors unfortunately are typically nonlinear and non-Gaussian in nature, which depend on many factors (see Ref. [7] for more details), and they ultimately limit the obtainable estimation performance using a TAM. Magnetometer calibration is often accomplished using batch methods, where an entire set of data must be stored to determine the unknown parameters. This process is often repeated many times during the lifetime of a spacecraft in order to ensure the best possible precision obtained from magnetometer measurements.

If an attitude is known accurately, then the magnetometer calibration problem is easy to solve. However, this is generally not the case. Fortunately, an attitude-independent scalar observation can be obtained using the norms of the body-measurement and geomagnetic-reference vectors. For the noise-free case, these norms are identical because the attitude matrix preserves the length of a vector. This process is also known as "scalar checking". Unfortunately, even for the simpler magnetometer-bias determination problem, the loss function to be minimized is quartic in nature. The most common technique to overcome this difficulty has been proposed by Gambhir, who applies a "centering" approximation to yield a quadratic loss function that can be minimized using simple linear least squares.[8] Alonso and Shuster expand upon Gambhir's approach by using a second step that employs the centered estimate as an initial value to an iterative Gauss-Newton method. Their algorithm, called "TWOSTEP",[9] has been shown to perform well when other algorithms fail due to divergence problems. Furthermore, Alonso and Shuster have extended this approach to perform a complete calibration involving biases as well as scale factors and non-orthogonality corrections.[6]

One of the current goals of modern-day spacecraft is the ability to perform onboard and autonomous calibrations in real time without ground support. The disadvantage of the TWOSTEP algorithm is the requirement of a batch of data, which cannot be performed in real time. The centering approximation is linear and can be made into a sequential (real-time) algorithm, which is shown in this paper. However, the centering approach has been shown to be suboptimal for many realistic cases,[6] which is also confirmed by the results shown in this paper. The main objective of this paper is to present and compare two sequential algorithms that are suitable for real-time applications. The first algorithm uses an extended Kalman filter approach that is developed with commonly employed estimation techniques. The second algorithm uses an Unscented filter approach that offers very good results for robust calibration when the initial conditions are poorly known. Experimental results using data obtained from the TRACE spacecraft show the validity of the new real-time algorithms to perform onboard and autonomous calibrations.

The organization of this paper is as follows: First, the attitude-independent observation model is summarized. Then, the centered linear algorithm for the solution of the complete magnetometer calibration problem is shown. This is extended to a sequential process, which can be used for real-time estimates. Next, a real-time algorithm based on the extended Kalman filter is derived, followed by an algorithm based on the Unscented filter. Finally, simulation and experimental results are shown.

MEASUREMENT MODEL AND COVARIANCE

In this section the TAM measurement model is summarized. Also, the attitude-independent observation as well as the covariance of the determined parameters are shown. More details on these concepts can be found in Ref. [6]. The magnetometer measurements can be modelled as

$$\mathbf{B}_k = (I_{3\times3} + D)^{-1}(\mathcal{O}^T A_k \mathbf{H}_k + \mathbf{b} + \boldsymbol{\epsilon}_k), \quad k = 1,\, 2,\, \ldots,\, N \tag{1}$$

where $\mathbf{B}_k$ is the measurement of the magnetic field by the magnetometer at time t_k, $\mathbf{H}_k$ is the corresponding value of the geomagnetic field with respect to an Earth-fixed coordinate system, A_k is the unknown attitude matrix of the magnetometer with respect to the Earth-fixed coordinates, D is an unknown fully-populated symmetric matrix of scale factors (the diagonal elements) and non-orthogonality corrections (the off-diagonal elements), $\mathcal{O}$ is an orthogonal matrix (see Ref. [6] for a discussion on the physical connotations of this matrix), $\mathbf{b}$ is the bias vector, and $\boldsymbol{\epsilon}_k$ is the measurement noise vector that is assumed to be a zero-mean Gaussian process with covariance Σ_k. Also, $I_{n\times n}$ is an $n \times n$ identity matrix. The goal of the full calibration problem is to estimate D and $\mathbf{b}$. We first define the following quantities:

$$E \equiv 2D + D^2 \tag{2a}$$

$$\mathbf{c} \equiv (I_{3\times3} + D)\mathbf{b} \tag{2b}$$

$$S_k \equiv \begin{bmatrix} B_{1_k}^2 & B_{2_k}^2 & B_{3_k}^2 & 2B_{1_k}B_{2_k} & 2B_{1_k}B_{3_k} & 2B_{2_k}B_{3_k} \end{bmatrix} \tag{2c}$$

$$\mathbf{E} \equiv \begin{bmatrix} E_{11} & E_{22} & E_{33} & E_{12} & E_{13} & E_{23} \end{bmatrix}^T \tag{2d}$$

An attitude-independent observation can be computed from

$$z_k \equiv ||\mathbf{B}_k||^2 - ||\mathbf{H}_k||^2 \tag{3a}$$

$$= L_k \boldsymbol{\theta}' - ||\mathbf{b}(\boldsymbol{\theta}')||^2 + v_k \tag{3b}$$

with

$$L_k \equiv \begin{bmatrix} 2\mathbf{B}_k^T & -S_k \end{bmatrix} \tag{4a}$$

$$\boldsymbol{\theta}' \equiv \begin{bmatrix} \mathbf{c} \\ \mathbf{E} \end{bmatrix} \tag{4b}$$

$$v_k \equiv 2[(I_{3\times3} + D)\mathbf{B}_k - \mathbf{b}]^T \boldsymbol{\epsilon}_k - ||\boldsymbol{\epsilon}_k||^2 \tag{4c}$$

The effective measurement noise, v_k, is approximately Gaussian with mean denoted by μ_k and variance denoted by σ_k^2, each given by

$$\mu_k \equiv E\left\{v_k\right\} = -\mathrm{Tr}(\Sigma_k) \tag{5a}$$

$$\sigma_k^2 \equiv E\left\{v_k^2\right\} - \mu_k^2 = 4[(I_{3\times3} + D)\mathbf{B}_k - \mathbf{b}]^T \Sigma_k [(I_{3\times3} + D)\mathbf{B}_k - \mathbf{b}] + 2\left(\mathrm{Tr}\,\Sigma_k^2\right) \tag{5b}$$

Note that the measurement variance is a function of the unknown parameters. Equation (3a) is used to compute the actual effective measurement, while Eq. (3b) represents the measurement model as a function of the unknown parameters E and $\mathbf{c}$.

Once E and $\mathbf{c}$ are determined, then a conversion from these parameters to D and $\mathbf{b}$ is required. This is accomplished by first decomposing E as

$$E = U\,V\,U^T \tag{6}$$

where U is an orthogonal matrix and V is a diagonal matrix with elements given by V_{11}, V_{22} and V_{33}. We define W to be a diagonal matrix with elements given by

$$W_{jj} = -1 + \sqrt{1 + V_{jj}}, \quad j = 1,\, 2,\, 3 \tag{7}$$

Then, the matrix D is given by

$$D = U\,W\,U^T \tag{8}$$

Also, $\mathbf{b}$ can be computed using Eq. (2b):

$$\mathbf{b} = (I_{3\times 3} + D)^{-1}\mathbf{c} \tag{9}$$

Another quantity of interest is the transformation of the covariance of $\boldsymbol{\theta'}$, denoted by $P_{\theta'\theta'}$, to the covariance of $\boldsymbol{\theta}$, denoted by $P_{\theta\theta}$, where

$$\boldsymbol{\theta} \equiv \begin{bmatrix} \mathbf{b} \\ \mathbf{D} \end{bmatrix} \tag{10a}$$

$$\mathbf{D} \equiv \begin{bmatrix} D_{11} & D_{22} & D_{33} & D_{12} & D_{13} & D_{23} \end{bmatrix}^T \tag{10b}$$

The covariance $P_{\theta'\theta'}$ is computed from a particular estimation algorithm. The covariance transformation is given by

$$P_{\theta\theta} = \left[\frac{\partial(\mathbf{b},\,\mathbf{D})}{\partial(\mathbf{c},\,\mathbf{E})}\right] P_{\theta'\theta'} \left[\frac{\partial(\mathbf{b},\,\mathbf{D})}{\partial(\mathbf{c},\,\mathbf{E})}\right]^T \tag{11}$$

where

$$\left[\frac{\partial(\mathbf{b},\,\mathbf{D})}{\partial(\mathbf{c},\,\mathbf{E})}\right] = \left[\frac{\partial(\mathbf{c},\,\mathbf{E})}{\partial(\mathbf{b},\,\mathbf{D})}\right]^{-1} = \begin{bmatrix} (I_{3\times 3} + D) & M_{cD}(\mathbf{b}) \\ 0_{6\times 3} & 2I_{6\times 6} + M_{ED}(\mathbf{D}) \end{bmatrix}^{-1} \tag{12}$$

with

$$M_{ED}(\mathbf{D}) = \begin{bmatrix} 2D_{11} & 0 & 0 & 2D_{12} & 2D_{13} & 0 \\ 0 & 2D_{22} & 0 & 2D_{12} & 0 & 2D_{23} \\ 0 & 0 & 2D_{33} & 0 & 2D_{13} & 2D_{23} \\ D_{12} & D_{12} & 0 & D_{11} + D_{22} & D_{23} & D_{13} \\ D_{13} & 0 & D_{13} & D_{23} & D_{11} + D_{33} & D_{13} \\ 0 & D_{23} & D_{23} & D_{13} & D_{12} & D_{22} + D_{33} \end{bmatrix} \tag{13}$$

and

$$M_{cD}(\mathbf{b}) = \begin{bmatrix} b_1 & 0 & 0 & b_2 & b_3 & 0 \\ 0 & b_2 & 0 & b_1 & 0 & b_3 \\ 0 & 0 & b_3 & 0 & b_1 & b_2 \end{bmatrix} \tag{14}$$

Also, $0_{m\times n}$ is an $m \times n$ matrix of zeros.

CENTERED ALGORITHM

The measurement model in Eq. (3b) is clearly nonlinear in the unknown parameter vector $\boldsymbol{\theta}'$. Therefore, linear least squares cannot be applied directly. However, it is possible to determine an approximate linear solution by applying a centering approach. First, the following weighted averages are defined:

$$\bar{L} \equiv \bar{\sigma}^2 \sum_{k=1}^{N} \frac{1}{\sigma_k^2} L_k \tag{15a}$$

$$\bar{z} \equiv \bar{\sigma}^2 \sum_{k=1}^{N} \frac{1}{\sigma_k^2} z_k \tag{15b}$$

$$\bar{\mu} \equiv \bar{\sigma}^2 \sum_{k=1}^{N} \frac{1}{\sigma_k^2} \mu_k \tag{15c}$$

where

$$\frac{1}{\bar{\sigma}^2} \equiv \sum_{k=1}^{N} \frac{1}{\sigma_k^2} \tag{16}$$

Next, the following centered variables are defined:

$$\tilde{L}_k \equiv L_k - \bar{L} \tag{17a}$$

$$\tilde{z}_k \equiv z_k - \bar{z} \tag{17b}$$

$$\tilde{\mu}_k \equiv \mu_k - \bar{\mu} \tag{17c}$$

Then, an approximation for the optimal estimate of $\boldsymbol{\theta}'$, denoted by $\tilde{\boldsymbol{\theta}}'^*$, is given by[6]

$$\tilde{\boldsymbol{\theta}}'^* = \tilde{P}_{\theta'\theta'} \sum_{k=1}^{N} \frac{1}{\sigma_k^2} (\tilde{z}_k - \tilde{\mu}_k) \tilde{L}_k^T \tag{18a}$$

$$\tilde{P}_{\theta'\theta'} = \left[\sum_{k=1}^{N} \frac{1}{\sigma_k^2} \tilde{L}_k^T \tilde{L}_k \right]^{-1} \tag{18b}$$

where $\tilde{P}_{\theta'\theta'}$ is the covariance of $\tilde{\boldsymbol{\theta}}'^*$. Equations (6)-(9) can now be used to determine D and $\mathbf{b}$. Also, Eq. (11) can be used to determine an approximation for the covariance of $\boldsymbol{\theta}^*$, replacing $P_{\theta'\theta'}$ with $\tilde{P}_{\theta'\theta'}$.

The approximate solution using Eq. (18) uses an entire batch of data. Since this solution is linear, then a sequential formulation can be derived that provides real-time estimates. A formal

derivation of this process can be found in Ref. [10]; we only present the final algorithm here. The sequential formulas for the averaged quantities in Eq. (15) are given by

$$\bar{L}_{k+1} = \frac{1}{\sigma_{k+1}^2 + \bar{\sigma}_k^2} \left(\sigma_{k+1}^2 \bar{L}_k + \bar{\sigma}_{k+1}^2 L_{k+1} \right) \tag{19a}$$

$$\bar{z}_{k+1} = \frac{1}{\sigma_{k+1}^2 + \bar{\sigma}_k^2} \left(\sigma_{k+1}^2 \bar{z}_k + \bar{\sigma}_{k+1}^2 z_{k+1} \right) \tag{19b}$$

$$\bar{\mu}_{k+1} = \frac{1}{\sigma_{k+1}^2 + \bar{\sigma}_k^2} \left(\sigma_{k+1}^2 \bar{\mu}_k + \bar{\sigma}_{k+1}^2 \mu_{k+1} \right) \tag{19c}$$

where

$$\frac{1}{\bar{\sigma}_{k+1}^2} = \frac{1}{\bar{\sigma}_k^2} + \frac{1}{\sigma_{k+1}^2} \tag{20}$$

Finally, the sequential formulas for $\tilde{\boldsymbol{\theta}}'^*$ and $\tilde{P}_{\theta'\theta'}$ are given by

$$\tilde{\boldsymbol{\theta}}'^*_{k+1} = K_k \tilde{\boldsymbol{\theta}}'^*_k + \frac{1}{\sigma_{k+1}^2} \left(\tilde{z}_{k+1} - \tilde{\mu}_{k+1} \right) \tilde{P}_{\theta'\theta'_{k+1}} \tilde{L}_{k+1}^T \tag{21a}$$

$$\tilde{P}_{\theta'\theta'_{k+1}} = K_k \tilde{P}_{\theta'\theta'_k} \tag{21b}$$

where the gain K_k is defined by

$$K_k \equiv I_{9\times 9} - \tilde{P}_{\theta'\theta'_k} \tilde{L}_{k+1}^T \left(\tilde{L}_{k+1} \tilde{P}_{\theta'\theta'_k} \tilde{L}_{k+1}^T + \sigma_{k+1}^2 \right)^{-1} \tilde{L}_{k+1} \tag{22}$$

Note that only an inverse of a scalar quantity is required in the sequential process. Also, an approach for determining σ_{k+1}^2 involves using the previous estimate in Eq. (5b). The solutions for $\tilde{\boldsymbol{\theta}}'^*_N$ and $\tilde{P}_{\theta'\theta'_N}$ can be shown to be equivalent to the batch solutions given by Eq. (18). The sequential process can be initialized using a small batch of data. A discussion on the observability of the centered estimate can be found in Ref. [11]. The TWOSTEP algorithm[9] uses the centered estimate as a starting value for a Gauss-Newton iteration (see Ref. [6] for more details), but this solution cannot be executed in real time.

KALMAN FILTER FORMULATION

In this section an extended Kalman filter (EKF) is derived to determine $\boldsymbol{\theta}'$ in real time. A summary of the EKF equations can be found in Refs. [12] and [13]. Since the vector $\boldsymbol{\theta}'$ is constant, then the state model is given by

$$\dot{\hat{\mathbf{x}}}(t) = \mathbf{0} \tag{23}$$

where $\hat{\mathbf{x}} \equiv \boldsymbol{\theta}'^*$, which is used to denote the optimal state estimate. The measurement model is given by

$$z_k = h(\mathbf{x}_k) + v_k \tag{24}$$

where $h(\mathbf{x}_k) \equiv L_k \boldsymbol{\theta}'_k - ||\mathbf{b}_k(\boldsymbol{\theta}'_k)||^2$ from Eq. (3b). Since no process noise appears in the state model of Eq. (23), then the updated quantities (state and covariance) are given by their respective propagated quantities. The EKF equations then reduce down to

$$\hat{\mathbf{x}}_{k+1} = \hat{\mathbf{x}}_k + K_k [z_k - h(\hat{\mathbf{x}}_k)] \tag{25a}$$

$$P_{k+1} = [I_{9\times 9} - K_k H_k(\hat{\mathbf{x}}_k)] P_k \tag{25b}$$

$$K_k = P_k H_k^T(\hat{\mathbf{x}}_k) \left[H_k(\hat{\mathbf{x}}_k) P_k H_k^T(\hat{\mathbf{x}}_k) + \sigma_k^2(\hat{\mathbf{x}}_k) \right]^{-1} \tag{25c}$$

where $P \equiv P_{\theta'\theta'}$. The state dependence of the measurement variance, σ_k^2, is shown through Eq. (5b). The 1×9 matrix $H(\mathbf{x})$ is the partial derivative of $h(\mathbf{x})$ with respect to $\mathbf{x}$. This quantity is given by

$$H(\mathbf{x}) = L - \frac{\partial ||\mathbf{b}(\boldsymbol{\theta}')||^2}{\partial \boldsymbol{\theta}'} \tag{26}$$

The partial derivatives of $||\mathbf{b}(\boldsymbol{\theta}')||^2$ are given by[6]

$$\frac{\partial ||\mathbf{b}(\boldsymbol{\theta}')||^2}{\partial c_m} = 2\left[(I_{3\times 3} + E)^{-1}\mathbf{c}\right]_m \tag{27a}$$

$$\frac{\partial ||\mathbf{b}(\boldsymbol{\theta}')||^2}{\partial E_{mn}} = -(2 - \delta_{mn})\left[(I_{3\times 3} + E)^{-1}\mathbf{c}\right]_m \left[(I_{3\times 3} + E)^{-1}\mathbf{c}\right]_n \tag{27b}$$

where $\left[(I_{3\times 3} + E)^{-1}\mathbf{c}\right]_m$ denotes the m^{th} element of $(I_{3\times 3} + E)^{-1}\mathbf{c}$, and δ_{mn} is the Kronecker symbol.

UNSCENTED FILTER FORMULATION

In this section a new approach, developed by Julier, Uhlmann and Durrant-Whyte,[14] is shown as an alternative to the extended Kalman filter. This approach, which they called the *Unscented filter* (UF), typically involves more computations than the extended Kalman filter, but has several advantages, including: 1) the expected error is lower than the extended Kalman filter, 2) the new filter can be applied to non-differentiable functions, 3) the new filter avoids the derivation of Jacobian matrices, and 4) the new filter is valid to higher-order expansions than the standard extended Kalman filter. The Unscented filter works on the premise that with a fixed number of parameters it should be easier to approximate a Gaussian distribution than to approximate an arbitrary nonlinear function. The filter presented in Ref. [14] is derived for discrete-time nonlinear equations, where the system model is given by

$$\mathbf{x}_{k+1} = \mathbf{f}(\mathbf{x}_k,\, \mathbf{w}_k,\, k) \tag{28a}$$

$$\mathbf{z}_k = \mathbf{h}(\mathbf{x}_k,\, \mathbf{v}_k,\, k) \tag{28b}$$

Note that a continuous-time model can always be written using Eq. (28a) through an appropriate numerical integration scheme. The vectors $\mathbf{w}_k$ and $\mathbf{v}_k$ are zero-mean Gaussian noise processes with covariances given by Q_k and R_k, respectively. The Kalman filter update equations are first rewritten as[15]

$$\hat{\mathbf{x}}_k^+ = \hat{\mathbf{x}}_k^- + K_k \boldsymbol{\upsilon}_k \tag{29a}$$

$$P_k^+ = P_k^- - K_k P_k^{\upsilon\upsilon} K_k^T \tag{29b}$$

where $\boldsymbol{\upsilon}_k$ is the *innovations process*, given by

$$\begin{aligned} \boldsymbol{\upsilon}_k &\equiv \mathbf{z}_k - \hat{\mathbf{z}}_k^- \\ &= \mathbf{z}_k - \mathbf{h}(\hat{\mathbf{x}}_k^-,\, k) \end{aligned} \tag{30}$$

The covariance of $\boldsymbol{\upsilon}_k$ is defined by $P_k^{\upsilon\upsilon}$. The gain K_k is computed by

$$K_k = P_k^{xz}(P_k^{\upsilon\upsilon})^{-1} \tag{31}$$

where P_k^{xz} is the cross-correlation matrix between $\hat{\mathbf{x}}_k^-$ and $\hat{\mathbf{z}}_k^-$.

The Unscented filter uses a different propagation than the standard extended Kalman filter. Given an $n \times n$ covariance matrix P, a set of order n points can be generated from the columns (or rows) of the matrices $\pm\sqrt{nP}$. The set of points is zero-mean, but if the distribution has mean $\boldsymbol{\mu}$, then simply adding $\boldsymbol{\mu}$ to each of the points yields a symmetric set of $2n$ points having the desired mean and covariance.[14] Due to the symmetric nature of this set, its odd central moments are zero, so its first three moments are the same as the original Gaussian distribution. This is the foundation for the Unscented filter. A complete derivation of this filter is beyond the scope of the present paper, so only the final results are presented here. Various methods can be used to handle the process noise and measurement noise in the Unscented filter. One approach involves augmenting the covariance matrix with

$$P_k^a = \begin{bmatrix} P_k^+ & P_k^{xw} & P_k^{xv} \\ (P_k^{xw})^T & Q_k & P_k^{wv} \\ (P_k^{xv})^T & (P_k^{wv})^T & R_k \end{bmatrix} \tag{32}$$

where P_k^{xw} is the correlation between the state error and process noise, P_k^{xv} is the correlation between the state error and measurement noise, and P_k^{wv} is the correlation between the process noise and measurement noise, which are all zero for most systems. Augmenting the covariance requires the computation of $2(q+l)$ additional sigma points (where q is the dimension of $\mathbf{w}_k$ and l is the dimension of $\mathbf{v}_k$, which does not necessarily have to be the same dimension, m, as the output in this case), but the effects of the process and measurement noise in terms of the impact on the mean and covariance are introduced with the same order of accuracy as the uncertainty in the state.

The general formulation for the propagation equations are given as follows. First, the following set of *sigma points* are computed:

$$\boldsymbol{\sigma}_k \leftarrow 2L \text{ columns from } \pm\gamma\sqrt{P_k^a} \tag{33a}$$

$$\boldsymbol{\chi}_k^a(0) = \hat{\mathbf{x}}_k^a \tag{33b}$$

$$\boldsymbol{\chi}_k^a(i) = \boldsymbol{\sigma}_k(i) + \hat{\mathbf{x}}_k^a \tag{33c}$$

where $L = n + q + l$ and $\hat{\mathbf{x}}_k^a$ is an augmented state defined by

$$\mathbf{x}_k^a = \begin{bmatrix} \mathbf{x}_k \\ \mathbf{w}_k \\ \mathbf{v}_k \end{bmatrix}, \quad \hat{\mathbf{x}}_k^a = \begin{bmatrix} \hat{\mathbf{x}}_k \\ \mathbf{0}_{q\times 1} \\ \mathbf{0}_{m\times 1} \end{bmatrix} \tag{34}$$

The parameter γ is given by

$$\gamma = \sqrt{L + \lambda} \tag{35}$$

where the composite scaling parameter, λ, is given by

$$\lambda = \alpha^2(L + \kappa) - L \tag{36}$$

The constant α determines the spread of the sigma points and is usually set to a small positive value (e.g. $1 \times 10^{-4} \leq \alpha \leq 1$).[16] Also, the parameter κ is usually given by $\kappa = 3 - L$. Efficient methods to compute the matrix square root can be found by using the Cholesky decomposition.[17]

If an orthogonal matrix square root is used, then the sigma points lie along the eigenvectors of the covariance matrix. Note that there are a total of $2L$ values for $\boldsymbol{\sigma}_k$ (the positive and negative square roots). The transformed set of sigma points are evaluated for each of the points by

$$\boldsymbol{\chi}_{k+1}(i) = \mathbf{f}(\boldsymbol{\chi}_k^x(i),\, \boldsymbol{\chi}_k^w(i),\, k) \tag{37}$$

where $\boldsymbol{\chi}_k^x(i)$ is a vector of the first n elements of $\boldsymbol{\chi}_k^a(i)$, and $\boldsymbol{\chi}_k^w(i)$ is a vector of the next q elements of $\boldsymbol{\chi}_k^a(i)$, with

$$\boldsymbol{\chi}_k^a(i) = \begin{bmatrix} \boldsymbol{\chi}_k^x(i) \\ \boldsymbol{\chi}_k^w(i) \\ \boldsymbol{\chi}_k^v(i) \end{bmatrix} \tag{38}$$

where $\boldsymbol{\chi}_k^v(i)$ is a vector of the last l elements of $\boldsymbol{\chi}_k^a(i)$, which will be used to compute the output covariance. The following weights are now defined:

$$W_0^{\text{mean}} = \frac{\lambda}{L+\lambda} \tag{39a}$$

$$W_0^{\text{cov}} = \frac{\lambda}{L+\lambda} + (1 - \alpha^2 + \beta) \tag{39b}$$

$$W_i^{\text{mean}} = W_i^{\text{cov}} = \frac{1}{2(L+\lambda)}, \quad i = 1,\, 2,\, \ldots,\, 2L \tag{39c}$$

where β is used to incorporate prior knowledge of the distribution (for Gaussian distributions $\beta = 2$ is optimal).

The predicted mean for the state estimate is calculated using a weighted sum of the points $\boldsymbol{\chi}_{k+1}^x(i)$, which is given by

$$\hat{\mathbf{x}}_{k+1}^- = \sum_{i=0}^{2L} W_i^{\text{mean}}\, \boldsymbol{\chi}_{k+1}^x(i) \tag{40}$$

The predicted covariance is given by

$$P_{k+1}^- = \sum_{i=0}^{2L} W_i^{\text{cov}} \left[\boldsymbol{\chi}_{k+1}^x(i) - \hat{\mathbf{x}}_{k+1}^-\right] \left[\boldsymbol{\chi}_{k+1}^x(i) - \hat{\mathbf{x}}_{k+1}^-\right]^T \tag{41}$$

The mean observation is given by

$$\hat{\mathbf{z}}_{k+1}^- = \sum_{i=0}^{2L} W_i^{\text{mean}}\, \boldsymbol{\zeta}_{k+1}(i) \tag{42}$$

where

$$\boldsymbol{\zeta}_{k+1}(i) = \mathbf{h}(\boldsymbol{\chi}_{k+1}^x(i),\, \boldsymbol{\chi}_{k+1}^v(i),\, k+1) \tag{43}$$

The output covariance is given by

$$P_{k+1}^{zz} = \sum_{i=0}^{2L} W_i^{\text{cov}} \left[\boldsymbol{\zeta}_{k+1}(i) - \hat{\mathbf{z}}_{k+1}^-\right] \left[\boldsymbol{\zeta}_{k+1}(i) - \hat{\mathbf{z}}_{k+1}^-\right]^T \tag{44}$$

Then the innovations covariance is simply given by

$$P_{k+1}^{vv} = P_{k+1}^{zz} \tag{45}$$

Finally the cross correlation matrix is determined using

$$P_{k+1}^{xz} = \sum_{i=0}^{2L} W_i^{\text{cov}} \left[\boldsymbol{\chi}_{k+1}^{x}(i) - \hat{\mathbf{x}}_{k+1}^{-}\right] \left[\boldsymbol{\zeta}_{k+1}(i) - \hat{\mathbf{z}}_{k+1}^{-}\right]^T \tag{46}$$

The filter gain is then computed using Eq. (31), and the state vector can now be updated using Eq. (29). Even though propagations on the order of $2n$ are required for the UF, the computations may be comparable to the EKF (especially if the continuous-time covariance equation needs to be integrated and a numerical Jacobian matrix is evaluated). Also, if the measurement noise, $\mathbf{v}_k$, appears linearly in the output (with $l = m$), then the augmented state can be reduced because the system state does not need to augmented with the measurement noise. In this case the covariance of the measurement error is simply added to the innovations covariance, with $P_{k+1}^{\upsilon\upsilon} = P_{k+1}^{zz} + R_{k+1}$. This can greatly reduce the computational requirements in the Unscented filter. Furthermore, a square root version of the UF is presented in Ref. [16] that avoids the need to re-factorize at each step.

The implementation of the UF for real-time magnetometer calibration proceeds as follows. Two approaches in the UF are presented here. The first uses the same concept for the measurement-error variance as with the EKF, where the UF measurement-error variance is given by $R_k = \sigma_k^2(\hat{\mathbf{x}}_k)$. In this approach the augmented state vector is simply given by the state, so that a decomposition of a 9×9 matrix is only required, with $P_k^a = P_k^+$. Since the state model estimate is given by $\dot{\hat{\mathbf{x}}}(t) = \mathbf{0}$, then $\hat{\mathbf{x}}_{k+1}^- = \hat{\mathbf{x}}_k^+$ and $P_{k+1}^- = P_k^+$, and Eqs. (40) and (41) are not needed (note: $Q_k = 0$). This significantly reduces the computational requirements in the UF. Equation (43) is computed using the measurement model in Eq. (3b), with $\mathbf{h}(\mathbf{x}_k,\, \mathbf{v}_k,\, k) \equiv L_k \boldsymbol{\theta}_k' - ||\mathbf{b}_k(\boldsymbol{\theta}_k')||^2 + v_k$. Also, the innovations covariance is given by $P_{k+1}^{\upsilon\upsilon} = P_{k+1}^{zz} + R_{k+1}$. Hence, the only essential difference between the EKF and UF formulations is in the computation of the innovations covariance, where the EKF uses a first-order expansion to compute this quantity, while the UF uses a nonlinear transformation to compute this quantity. The second approach for the UF uses the measurement noise model of Eq. (3b) with an augmented vector given by the state and $\boldsymbol{\epsilon}$ in Eq. (4c). The augmented covariance is now given by

$$P_k^a = \begin{bmatrix} P_k^+ & 0_{9\times 3} \\ \\ 0_{3\times 9} & \Sigma_k \end{bmatrix} \tag{47}$$

Therefore, a decomposition of a 12×12 matrix is now required. Again, since the state model estimate is given by $\dot{\hat{\mathbf{x}}}(t) = \mathbf{0}$, then $\hat{\mathbf{x}}_{k+1}^- = \hat{\mathbf{x}}_k^+$ and $P_{k+1}^- = P_k^+$, and Eqs. (40) and (41) are not needed. Also, the innovations covariance is computed using Eqs. (44) and (45) in this approach. In the strictest sense this approach is more optimal than the first approach because the effect of the nonlinear-appearing measurement noise is directly used in the UF. But, the computational requirements are vastly increased due to the decomposition of a higher dimensional augmented matrix.

SIMULATION AND EXPERIMENTAL RESULTS

In this section results of the EKF and UF formulations are shown using both simulated and experimental data. The simulated spacecraft is modelled after the Tropical Rainfall Measurement Mission (TRMM) spacecraft. This is an Earth-pointing spacecraft (spinning about its y-axis) in low-Earth orbit (currently near-circular at 402 km), with an inclination of 35°. The attitude

Table 1 Simulation Results

	Truth	TWOSTEP	Centered	EKF	UF
b_1	50 mG	49.9620 ± 0.4320	49.9700 ± 0.5525	49.4029 ± 2.2625	49.7289 ± 0.4328
b_2	30 mG	29.8174 ± 0.4258	29.5937 ± 5.5779	19.5297 ± 2.2044	29.4657 ± 0.3598
b_3	60 mG	60.0331 ± 0.3165	60.0456 ± 0.3165	50.3248 ± 1.2340	59.4561 ± 0.2331
D_{11}	0.05	0.0500 ± 0.0001	0.0500 ± 0.0001	0.0492 ± 0.0008	0.0499 ± 0.0001
D_{22}	0.10	0.0993 ± 0.0014	0.0988 ± 0.0123	0.0736 ± 0.0075	0.0949 ± 0.0013
D_{33}	0.05	0.0500 ± 0.0001	0.0500 ± 0.0001	0.0481 ± 0.0004	0.0499 ± 0.0001
D_{12}	0.05	0.0499 ± 0.0010	0.0499 ± 0.0011	0.0313 ± 0.0051	0.0486 ± 0.0010
D_{13}	0.05	0.0499 ± 0.0001	0.0499 ± 0.0001	0.0440 ± 0.0006	0.0495 ± 0.0002
D_{23}	0.05	0.0501 ± 0.0007	0.0501 ± 0.0007	0.0287 ± 0.0030	0.0487 ± 0.0006

determination system consists of an Earth Sensor Assembly (ESA), a TAM, Digital Sun Sensors (DSS), Coarse Sun Sensors, and gyroscopic rate sensors. Currently, the ESA data is unreliable, so only the TAM and DSS are used as attitude sensors combined with gyros in an EKF (see Ref. [18] for more details). The geomagnetic field is simulated using a 10^{th}-order International Geomagnetic Reference Field model.[7] The magnetometer-body and geomagnetic-reference vectors for the simulated runs each have a magnitude of about 500 milliGauss (mG). The measurement noise is assumed to be white and Gaussian, and the covariance is taken to be isotropic with a standard deviation of 0.5 mG. The measurements are sampled every 10 seconds over an 8-hour span. The true values for the bias $\mathbf{b}$ and elements of the D matrix are shown in Table 1. Large values for the biases are used to test the robustness of the EKF and UF algorithms.

Thirty runs have been executed, which provide a Monte-Carlo type simulation. Shown in Table 1 are the averaged batch solutions given by the TWOSTEP and centered algorithms, each with their maximum deviations obtained. Since the TWOSTEP approach is the most rigorous, all comparisons are made with respect to this algorithm. The centered algorithm does a fairly good job at estimating all parameters, with the exception of b_2. This parameter corresponds to the least observable variable, which results in a wide variation from the averaged value.

The EKF and UF are both executed at time $t = 0$ using initial conditions of zeros for all states. The initial covariance matrix is diagonal, given by

$$P_0 = \begin{bmatrix} 500 I_{3\times 3} & 0_{3\times 6} \\ 0_{6\times 3} & 0.001 I_{6\times 6} \end{bmatrix} \tag{48}$$

This assumes a 3σ bound on the initial bias estimates to be about 70 mG and a 3σ bound on the initial estimates for the elements of the D matrix to be about 0.1. The parameters used in the UF are $\alpha = 0.1$, $\beta = 2$, $\kappa = 3 - L$, and $L = 9$ when the 9×9 matrix decomposition approach is used ($L = 12$ for the augmented approach). The two UF approaches (one uses the current state estimate in the measurement-error variance calculation, which requires a 9×9 matrix decomposition, while the other appends the state vector to include the measurement noise, which requires a 12×12 matrix

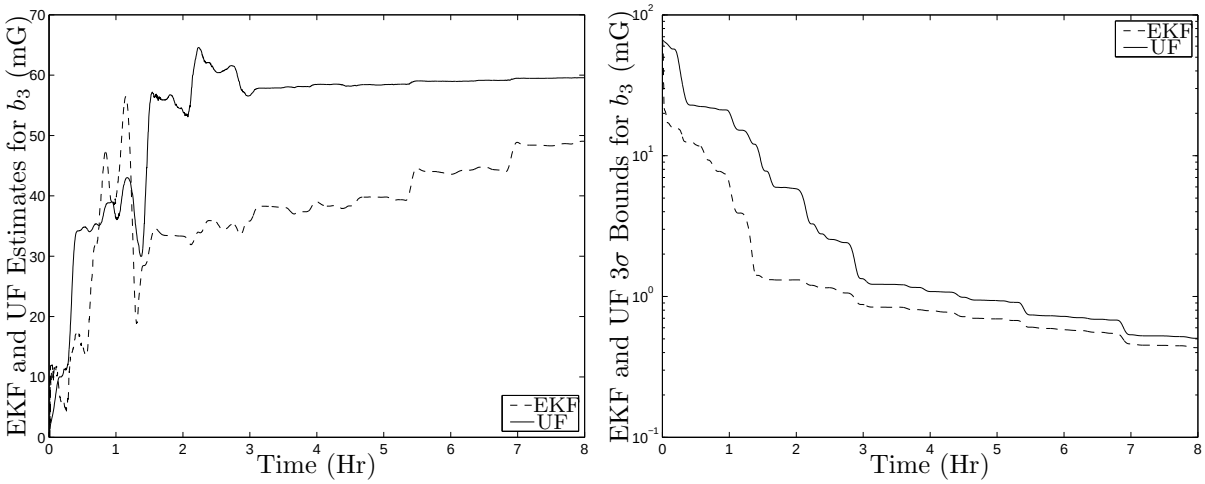

(i) EKF and UF Estimates **(ii)** 3σ Bounds

Figure 1 EKF and UF Estimates and 3σ Bounds for the Parameter b_3

decomposition) give identical results. Therefore, no apparent advantages to using the augmented approach in the UF is seen. The EKF and UF solutions at the final time are shown in Table 1. The EKF does not converge to the correct solution for many of the parameters, while the UF gave results that are just as good as the TWOSTEP solutions. Also, the maximum deviations for the UF are much smaller than for the EKF and centered algorithm.

Figure 1(i) shows the EKF and UF estimates for the parameter b_3. The EKF does not converge to the correct solution during the 8-hour simulated run. This is due to the fact that the first-order approximation in the EKF does not adequately capture the large initial errors. The biggest concern with the EKF solutions is the confidence of the results dictated by the 3σ bounds, with b_3 shown in Figure 1(ii). In fact, this plot shows that the EKF is performing better than the UF. This can certainly provide some misleading results. However, unlike the EKF, the maximum deviations associated with the UF shown in Table 1 are within the 3σ bounds for all the parameters. This indicates that the UF is performing in an optimal manner. But, the UF algorithm comes with a computational cost, mainly due to the covariance decomposition. Our experience has shown that the UF algorithm is about 2 times slower than the EKF algorithm. Still, the performance enhancements of the UF over the EKF may outweigh the increased computational costs.

Next, experimental results from the TRACE spacecraft are shown. This is an Sun-synchronous spacecraft in low-Earth orbit (currently near-circular at 402 km). The attitude determination system consists of a TAM, DSS and gyroscopic rate sensors. The data collected for the spacecraft is given during an inertial pointing mode. As discussed previously the errors associated with the geomagnetic field model are typically nonlinear and non-Gaussian in nature. This violates the assumptions for all the estimators shown in this paper. We still assume that the measurement noise is white and Gaussian, but the standard deviation is now increased to a value of 3 mG, which bounds the errors in a practical sense. The measurements are sampled every 3 seconds over a 6-hour span. Figure 2(i) shows the magnetic field reference for all axes, and Figure 2(ii) shows the actual TAM measurements.

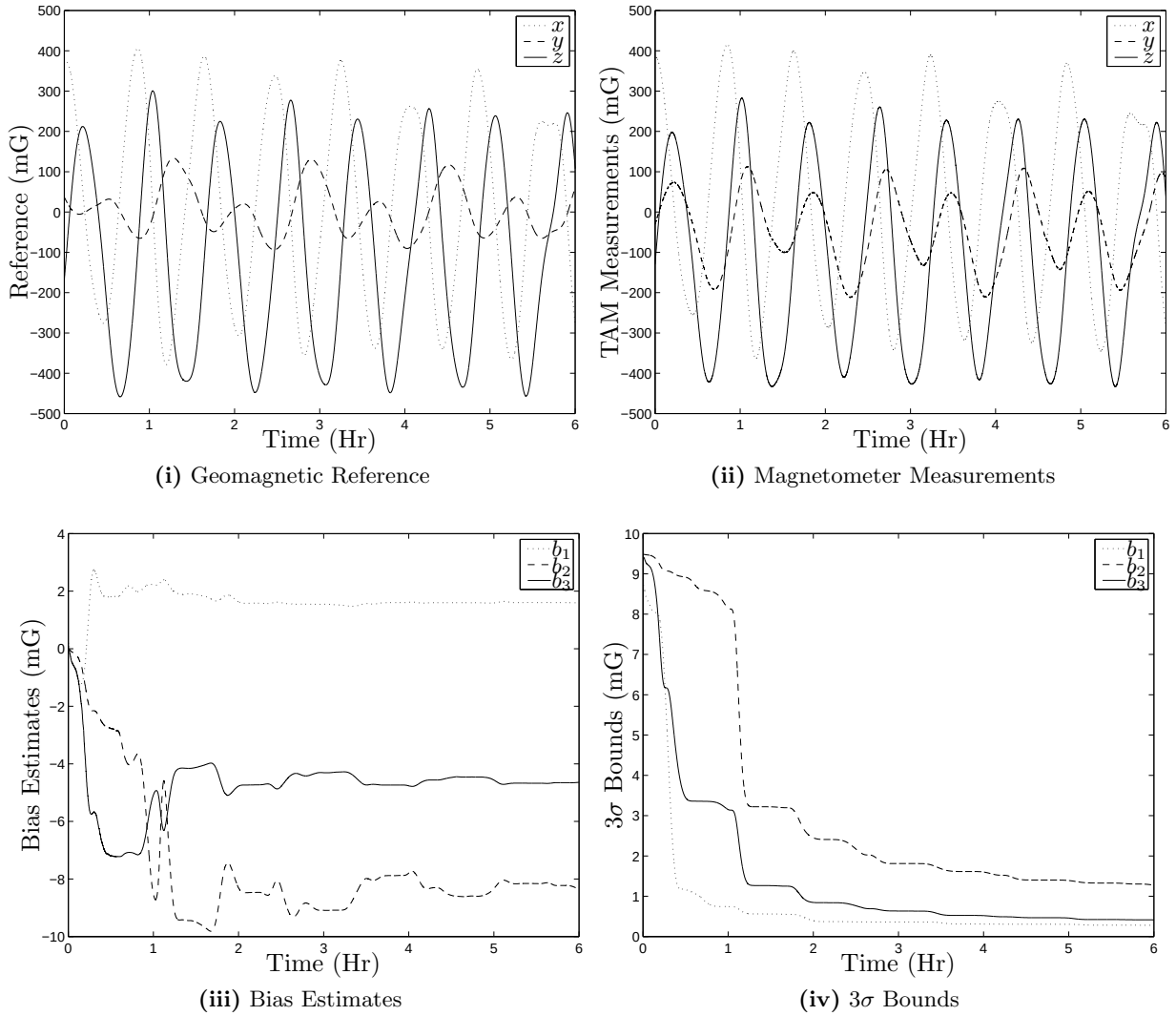

(i) Geomagnetic Reference **(ii)** Magnetometer Measurements

(iii) Bias Estimates **(iv)** 3σ Bounds

Figure 2 Reference and Measurements from TRACE, and Bias Estimates and 3σ Bounds

The EKF and UF are both executed at time $t = 0$ using initial conditions of zeros for all states. The initial covariance matrix is diagonal, given by

$$P_0 = \begin{bmatrix} 10I_{3\times 3} & 0_{3\times 6} \\ \\ 0_{6\times 3} & 0.001I_{6\times 6} \end{bmatrix} \tag{49}$$

This assumes a 3σ bound on the initial bias estimates to be about 10 mG and a 3σ bound on the initial estimates for the elements of the D matrix to be about 0.1. The parameters used in the UF are $\alpha = 0.1$, $\beta = 2$, $\kappa = 3 - L$, and $L = 9$ when the 9×9 matrix decomposition approach is used ($L = 12$ for the augmented approach). Once again no advantages to using the augmented approach in the UF are seen. For the experimental data the solutions obtained using TWOSTEP, the EKF and UF algorithms are nearly identical. This is most likely due to the well-behaved nature of the data (i.e., the calibration errors are small). However, the sequential centered algorithm gave

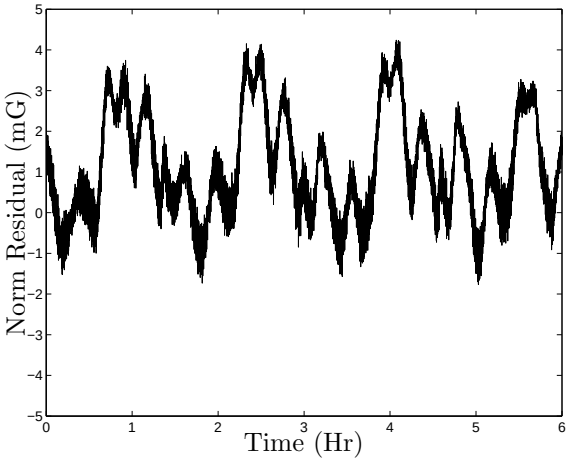

Figure 3 Norm Residual Between Body Estimates and Reference Vectors

slightly different results, which indicates that this approach is not truly optimal, even when small errors are present. The centered algorithm final results are given by

$$\mathbf{b}^* = \begin{bmatrix} 1.4007 & -8.7350 & -3.7927 \end{bmatrix}^T \tag{50a}$$

$$D^* = \begin{bmatrix} 0.0086 & 0.0437 & 0.0065 & 0.0006 & 0.0035 & -0.0120 \end{bmatrix}^T \tag{50b}$$

The TWOSTEP, EKF and UF final results are given by

$$\mathbf{b}^* = \begin{bmatrix} 1.6056 & -8.4140 & -4.6123 \end{bmatrix}^T \tag{51a}$$

$$D^* = \begin{bmatrix} 0.0123 & 0.0181 & 0.0040 & -0.0005 & 0.0038 & -0.0019 \end{bmatrix}^T \tag{51b}$$

These results indicate that the EKF and UF algorithms should be used over the sequential centered algorithm for real-time calibration purposes. Figure 2(iii) shows EKF estimates for the bias vector $\mathbf{b}$. Another advantage of a real-time approach is the convergence properties of the particular estimator. From Figure 2(iii) good convergence is seen for all the parameters, which indicates that the calibration parameters are well behaved (i.e., truly constant in a practical sense). Figure 2(iv) shows the 3σ bounds for the bias estimates. This at least qualitatively indicates that good parameter estimates are achieved since these bounds are fairly small compared to the TAM measurements. Similar results are obtained for the D matrix parameters.

An investigation of the residuals between the norm of the estimated vector, using the calibrated parameters, and the geomagnetic-reference vector is useful to check the consistency of the results. A plot of this residual is shown in Figure 3. From this plot the residuals are slightly biased by about 2 mG and have some non-Gaussian components. This clearly shows the nonlinear and non-Gaussian nature of the geomagnetic field model. A spectrum analysis shows the presence of sinusoidal motions with periods equivalent to the orbital period ($\approx$ 90 min) and higher-order harmonics (see Ref. [19] for a model of this process). Still, the residuals are small enough to indicate that good results are obtained from the real-time calibration algorithms developed in this paper.

CONCLUSIONS

In this paper two new real-time algorithms based on the extended Kalman filter and Unscented filter were developed for the calibration of three-axis magnetometers. Also, a sequential algorithm was shown that was based on a linear least squares approach using a centering approximation. Two different approaches have also been shown in the Unscented filter design. One uses the current state estimate in the measurement-error variance calculation, which requires a 9×9 matrix decomposition, while the other appends the state vector to include the nonlinear-appearing measurement noise, which requires a 12×12 matrix decomposition. Simulation and experimental results indicated that for this problem, both Unscented filter approaches gave identical results. So appending the state vector is not required, which significantly reduces the computational requirements in the Unscented filter. Simulation test cases also showed that the performance of the Unscented filter is significantly better than the standard extended Kalman filter and sequential centered algorithm for large initialization errors. Experimental results indicated that the EKF and UF algorithms should be used over the sequential centered algorithm for real-time calibration purposes, even when small errors are present. However, the Unscented filter algorithm is recommended for actual implementation when computational requirements are not burdensome.

REFERENCES

1. B. T. Blaylock, "Magnetometers," *Spacecraft Attitude Determination and Control*, edited by J. R. Wertz, chap. 6.3, Kluwer Academic Publishers, The Netherlands, 1978, pp. 180–184.

2. M. L. Psiaki, F. Martel, and P. K. Pal, "Three-Axis Attitude Determination via Kalman Filtering of Magnetometer Data," *Journal of Guidance, Control, and Dynamics*, Vol. 13, No. 3, May-June 1990, pp. 506–514.

3. M. Challa and G. Natanson, "Effects of Magnetometer Calibration and Maneuvers on Accuracies of Magnetometer-Only Attitude and Rate Determination," *Proceedings of the AAS/GSFC 13th International Symposium on Space Flight Dynamics*, Vol. 1, (NASA/CP-1998-206858/VOL1) NASA-Goddard Space Flight Center, Greenbelt, MD, May 1998, pp. 389–401.

4. J. K. Deutschmann and I. Bar-Itzhack, "Evaluation of Attitude and Orbit Estimation Using Actual Earth Magnetic Field Data," *Journal of Guidance, Control, and Dynamics*, Vol. 24, No. 3, May-June 2001, pp. 616–623.

5. J. Jung and M. L. Psiaki, "Tests of Magnetometer/Sun-Sensor Orbit Determination Using Flight Data," *Journal of Guidance, Control, and Dynamics*, Vol. 25, No. 3, May-June 2002, pp. 582–590.

6. R. Alonso and M. D. Shuster, "Complete Linear Attitude-Independent Magnetometer Calibration," *to appear in the Journal of the Astronautical Sciences*, 2003.

7. R. A. Langel, "The Main Field," *Geomagnetism*, edited by J. A. Jacobs, Academic Press, Orlando, FL, 1987, pp. 249–512.

8. R. Alonso and M. D. Shuster, "Attitude-Independent Magnetometer-Bias Determination: A Survey," *to appear in the Journal of the Astronautical Sciences*, 2003.

9. R. Alonso and M. D. Shuster, "A New Algorithm for Attitude-Independent Magnetometer Calibration," *Proceedings of the Flight Mechanics/Estimation Theory Symposium*, (NASA/CP-3265) NASA-Goddard Space Flight Center, Greenbelt, MD, May 1994, pp. 513–527.

10. J. L. Crassidis, F. L. Markley, and E. G. Lightsey, "Global Positioning System Integer Ambiguity Resolution Without Attitude Knowledge," *Journal of Guidance, Control, and Dynamics*, Vol. 22, No. 2, March-April 1999, pp. 212–218.

11. R. Alonso and M. D. Shuster, "Centering and Observability in Attitude-Independent Magnetometer-Bias Determination," *to appear in the Journal of the Astronautical Sciences*, 2003.

12. A. Gelb, editor, *Applied Optimal Estimation*, The MIT Press, Cambridge, MA, 1974.

13. J. L. Crassidis and J. L. Junkins, *Optimal Estimation of Dynamic System*, CRC Press, Boca Raton, FL, to be published.

14. S. J. Julier, J. K. Uhlmann, and H. F. Durrant-Whyte, "A New Method for the Nonlinear Transformation of Means and Covariances in Filters and Estimators," *IEEE Transactions on Automatic Control*, Vol. AC-45, No. 3, March 2000, pp. 477–482.

15. Y. Bar-Shalom and T. E. Fortmann, *Tracking and Data Association*, Academic Press, Boston, MA, 1988.

16. E. Wan and R. van der Merwe, "The Unscented Kalman Filter," *Kalman Filtering and Neural Networks*, edited by S. Haykin, chap. 7, Wiley, 2001.

17. G. H. Golub and C. F. Van Loan, *Matrix Computations*, The Johns Hopkins University Press, Baltimore, MD, 2nd ed., 1989.

18. S. F. Andrews and S. Bilanow, "Recent Flight Results of the TRMM Kalman Filter," *AIAA Guidance, Navigation, and Control Conference*, Monterey, CA, Aug. 2002, AIAA-2002-5047.

19. J. L. Crassidis, S. F. Andrews, F. L. Markley, and K. Ha, "Contingency Designs for Attitude Determination of TRMM," *Proceedings of the Flight Mechanics/Estimation Theory Symposium*, (NASA/CP-3299) NASA-Goddard Space Flight Center, Greenbelt, MD, May 1995, pp. 419–433.